

Aiding and Opposing Re-circulating Mixed Convection Flows in a Square Vented Enclosure



Hayder A. Dhahad^a, Gazy F. Al-Sumaily^{a,b,*}, Wissam H. Alawee^a, Mark C. Thompson^b

^a Workshop and Training Centre, University of Technology, Baghdad, Iraq

^b Fluids Laboratory for Aeronautical and Industrial Research (FLAIR), Department of Mechanical and Aerospace Engineering, Monash University, Victoria 3800, Australia

ARTICLE INFO

Keywords:

Mixed convection
Aiding flow
Opposing flow
Jet flow
and Vented enclosure

ABSTRACT

A numerical study is performed to investigate mixed convective flow in a vertically vented square enclosure with heating or cooling one of the vertical walls and the other three walls are insulated. This study is conducted to analyse and clarify the intricate interaction between the buoyancy-induced flow and the pressure-driven external flow in a vertical upward laminar air jet for both assisting and opposing buoyancy situations. The approach of spectral-element that is introduced as a finite-element method with high-order Lagrange polynomials as interpolating functions, is applied to discretise unsteady Navier-Stokes, continuity and energy equations, and for calculating the velocity and temperature fields. The numerical solutions are obtained for air having a Prandtl number of ($Pr = 0.7$) and for buoyancy parameters which cover the whole mixed convection region, ranging from pure forced convection with a Reynolds number ranging between ($10 \leq Re \leq 350$) to pure free convection with a Richardson number ranging between ($0 \leq Ri \leq 30$), with a single dimensionless enclosure size. The results reveal that the flow and thermal patterns can be significantly influenced by both aiding and opposing buoyancies. Also, the mean heat transfer rates increase with increasing either the buoyancy force Richardson number or the forced flow Reynolds number in assisting flows. However, in opposing flows, it is found that the mean heat transfer rates decrease with increasing the buoyancy effects for small to moderate ($Ri \leq 2$) but, they begin rising for higher Richardson number when the free convection starts domination the flow.

1. Introduction

The fundamental challenge of designing more compact electronic products is thermal management. The quantity of heat generated within the integrated electronic circuit boards with the increase of package density accumulates and potentially damages the electronic components. Such overheating ambience shortens the life expectancy and can also be the primary cause of a product failure. Therefore, the thermal behaviour of such components always requires further attention and cannot be disregarded. Thus, creating a reliable and effective cooling technique to perform a high performance method of cooling that satisfies the heat dissipation requirements in such increasingly small electronic devices is a crucial demand for researchers in science and engineering. Among the techniques is the use of passive strategies, such as the obstacles and fins placement, porous media, utilising generators of vortex, or by lid-driving cavities, the use of active strategies, such as the suction and/or fluid blowing, the employment of external or local forcing, and the use of nanofluids, like the developed colloidal solutions

via the nanoparticles of silica carbides, metal oxides or metals. However, the air-cooling systems are considered as an essential cooling medium for electronic systems because of its simplicity in design and low cost of maintenance services. It is for such reason that the convective enclosure flow progresses to motivate and attract the concern of several researchers who aim to profound their awareness of such field for enhancing the transfer of heat in the aforementioned uses.

One of the most important forms of fluid flow and heat transfer in enclosures is the mixed convection that describes the operation of thermal energy transfer in fluids, where both free and forced convection impacts are of equivalent order. The complicated physical phenomena associated with the mixed convection driven by a combination of shear and buoyancy forces inside enclosures have been searched and discussed widely and is fairly well realised. The considerable efforts in previous studies have been devoted to modelling and simulating such a problem into side wall sliding lid-driven rectangular or square enclosures of horizontal [1–4], vertical [5–8] or inclined [9–12] one or more sides moving and for many pertinent parameters.

* Corresponding author.

E-mail addresses: 10592@uotechnology.edu.iq (H.A. Dhahad), gazy.alsumaily@monash.edu (G.F. Al-Sumaily), 20046@uotechnology.edu.iq (W.H. Alawee), mark.thompson@monash.edu (M.C. Thompson).

<https://doi.org/10.1016/j.tsep.2020.100577>

Nomenclature*Nomenclature*

| | |
|-----------|---|
| c_p | Specific heat capacity, (J/kg.K). |
| d | Enclosure inlet slot or outlet vent width, (m). |
| Gr | Grashof number, ($Gr = g \cdot \beta \cdot H^3 \cdot (T_w - T_o)/\nu^2$). |
| h | Coefficient of local convective heat transfer, ($W/m^2.K$). |
| H | Enclosure height, (m). |
| k | Thermal conductivity, ($W/m.K$). |
| n | Normal direction to the heat wall surface. |
| N | Number of internal nodes. |
| Nu_{av} | Surface-average Nusselt number. |
| Nu_l | Local mean-time surface-average Nusselt number. |
| Nu_m | Time- and surface-average Nusselt number. |
| p | Pressure, (N/m^2). |
| P | Dimensionless pressure, ($P = p/\rho \cdot \nu_o^2$). |
| Pr | Prandtl number, ($Pr = \nu/\alpha$). |
| Re | Reynolds number, ($Re = \nu_o \cdot H/\nu$). |
| Ri | Richardson number, ($Ri = Gr/Re^2$). |
| T | Temperature, ($^{\circ}C$). |
| t | Time, (sec). |
| u | Horizontal velocity, (m/s). |

| | |
|--------|--|
| U | Dimensionless horizontal velocity, ($U = u/\nu_o$). |
| ν | Vertical velocity, (m/s). |
| V | Dimensionless vertical velocity, ($V = \nu/\nu_o$). |
| x, y | Cartesian coordinates, (m). |
| X, Y | Dimensionless Cartesian coordinates, ($X = x/H, Y = y/H$). |

Greek symbols

| | |
|----------|--|
| α | Thermal diffusivity, (m^2/s). |
| β | Volumetric expansion coefficient, ($1/^{\circ}C$). |
| θ | Dimensionless temperature, ($\theta = (T - T_o)/(T_w - T_o)$). |
| ρ | Density, (kg/m^3). |
| μ | Dynamic viscosity, ($kg \cdot m^{-1} \cdot s^{-1}$). |
| ν | Kinematic viscosity, (m^2/s). |
| τ | Dimensionless time. |

Subscripts

| | |
|------|--------------------------------|
| av | Surface-average. |
| l | Local. |
| m | Time-mean and surface-average. |
| o | Inlet condition. |
| w | Wall. |

Mixed convection in an open-ended cavity structures embedded in horizontal or vertical channels, having a localised heat source or having a heated sidewall has received fair interest in the literature by, for example, [13–18], with stressing on the location influences of the heat source inside the cavity, and aspect ratio of the cavity on the interaction between the flow of free convection induced inside the cavity and the forced flow in the channel. The primary purpose of their investigations is to realise the bases of different cooling strategies and to accomplish a great effective cooling way that satisfies the heat dissipation demands of the electronic equipment with particular shapes. However, mixed convection flow in vented enclosures has received relatively less attention. Through supplying a vent and an inlet, the states of forced convection can be exploited within an enclosure. The interaction between the externally induced airflow and the free convection resulting from the buoyancy forces that stem from one or many elements used for heating in the enclosure performs a substantial role in designing the electronic devices. The works of [19–21] investigated the mixed convection from a single or multiple split heaters placed in a ventilated cavity. Radhakrishnan et al. [19] examined the effect of a single heater location at various positions, namely bottom, top and middle region, for location optimisation in order to have maximum cooling of heat generating element. They also studied the impact of the heater orientation in horizontal and inclined positions and found out that the horizontal position displays higher rate of heat transfer compared to inclined one. Radhakrishnan et al. [20] tested temperature distributions around multiple heaters in a staggered arrangement for power management among them. It was seen that the coolest heaters within the flow can be loaded most for maximum total heat dissipation and minimum temperature deviation from a targeted value. While, Chamkha et al. [21] checked the influences of the location and the aspect ratio of square heat source positioned at the centre of an air-ventilated cavity. They reported that these two parameters play significant roles in the flow and temperature distributions.

On the subject of laminar mixed convection in a horizontally vented cavity without separated heated body, Papanicolaou and Jaluria [22,23] conducted numerical studies to investigate this problem in horizontal square adiabatic enclosures with a localised heat source introduced within the interior walls. Their efforts were directed to analyse the influence of heat source location for different in- and out-flow

openings for obtaining an optimal position for better cooling. It was found that putting the heat source on the vertical right wall is the greater desirable place for cooling, and more improvement can be acquired by placing the outflow opening near the bottom of the perpendicular wall. A related investigation of mixed convection in a horizontal rectangular cavity partially divided by a conductive vertical baffle protruding from the ceiling or the floor, and differentially heated by a localised heat source, was numerically investigated by Hsu et al. [24]. Results were acquired for several positions of divider, the outflow opening, and the source of heat. They indicated that the higher rate of heat dissipated can be accomplished by locating the outflow opening lower of the vertical wall, and the cooling performance is enhanced if the source of heat is placed in the proximity of cold inlet jet. Laminar mixed convection in a horizontal vented cavity subjected to a solar radiation heat flux from the left sidewall and submitted to an either opposing or aiding cold stream jet was investigated in study of Raji and Hasnaoui [25]. Two enclosure configurations, BB (Bottom-Bottom) and BT (Bottom-Top), were examined. It was found that the BB configuration is not beneficial for heat discharge, as it provides higher

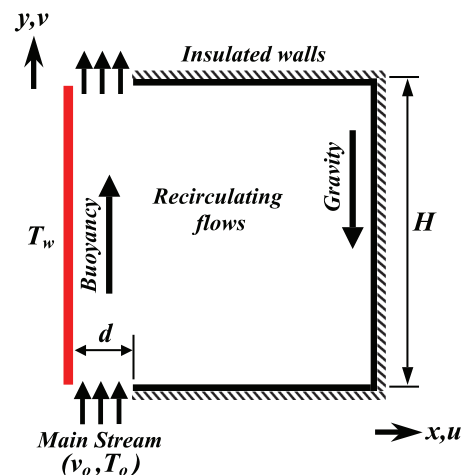


Fig. 1. The used geometric parameters and coordinate system.

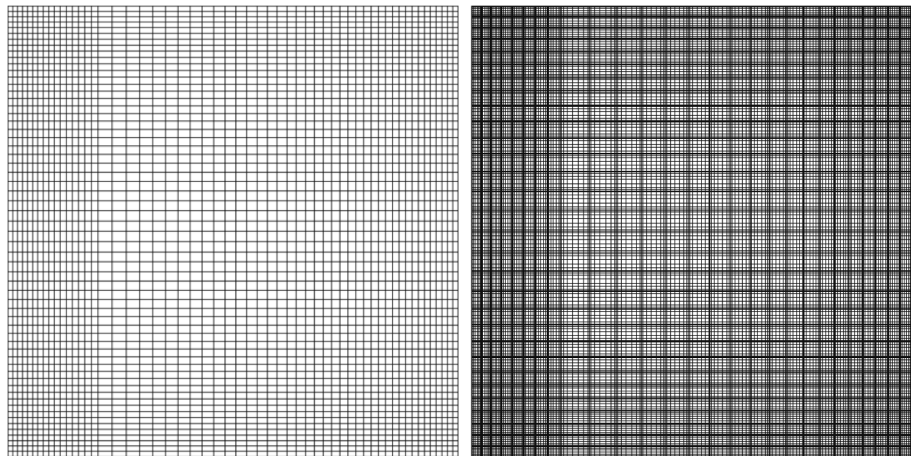


Fig. 2. (Left) Typical spectral macro-elements employed for the simulations. (Right) Elements are further subdivided into (8x8) internal node points.

temperature values, which lead to an uncomfortable thermal zone for occupation. Singh and Sharif [26] examined the mixed convective air-cooling of a horizontal rectangular enclosure with variously heated vertical sidewalls and keeping the horizontal walls insulated. They considered six different inlet and exit placement configurations to optimise their relative locations in order to have a higher efficient cooling by maximising the heat dissipation rate and decreasing the bulk temperature within the cavity. They observed that the extreme cooling efficiency can be attained if the inflow opening is kept close to the bottom of cold wall, while the outflow opening is positioned close the

top of hot wall. The works of [27,28] investigated the problem of mixed convection in a multiple ventilated cavity with double inlet slots positioned close to the tops of both upright walls and double outlet vents placed close to the bottoms of them. In the first study, the traits of transformation from the stable to chaotic flow were analysed for different inlet flow angles. The results revealed that, as Richardson number increases, a change from the steady-state to the periodic oscillatory-state flow behaviour and then to the non-periodic state is observed. It was also revealed that the horizontally directed inlet flow is the most unstable situation on the self-sustained oscillatory convective

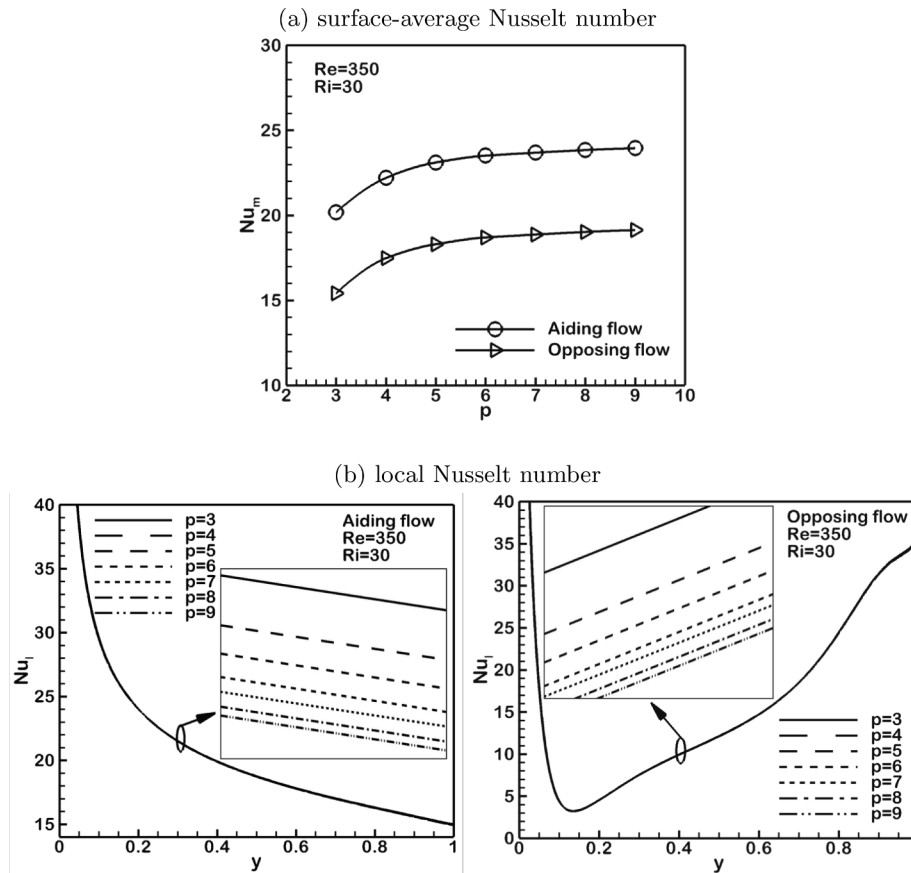


Fig. 3. Study of grid resolution of the calculation domain for both aiding and opposing flows, at two highest values of Reynolds number $Re = 350$ and Richardson number $Ri = 30$. This is conducted via changing the interpolation polynomial order p within the range of (3–9), whilst preserving the same layout of macro-element.

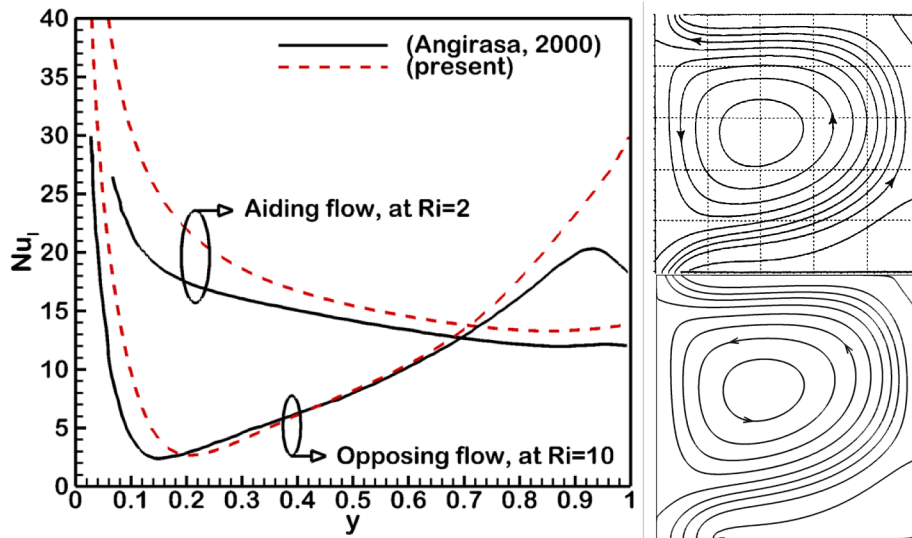


Fig. 4. The comparison between two numerical models: The current model and that employed by Angirasa [31] for the mixed convection flow in an enclosure, (Left) for the variation of local Nusselt number of aiding flow at $Ri = 2$ and opposing flow at $Ri = 10$, and (Right) for the streamlines of opposing flow at $Ri = 2$, (Top) predicted by Angirasa [31] and (bottom) predicted by the present code.

flow motion. Whereas, the second study considered the horizontal pulsating inlet flows for a range of Grashof, Reynolds and Strouhal numbers for the purpose of analysing the complex interaction between the inertial and buoyancy forces in the pulsatile flow. Lounes et al. [29] investigated mixed convection inside four configurations of ventilated cavities with different supply and exhaust ports. Each cavity configuration is provided with two ports: an inlet port for introducing fresh air, and an outlet port to extract hot air. They found out that the flow

configuration when the inlet is at the top and the outlet at the bottom of the left vertical wall gives a better ventilation effectiveness for temperature distribution.

For the case of mixed convection in a vertical vented cavity, the results are rather limited and only reported by [30–32], for evaluating the characteristics of aiding and opposing buoyant flows in vertical downward/upward inflow jets. Kumar and Yuan [30] examined the hot and cold vertical downward jets impinging from one end of the top

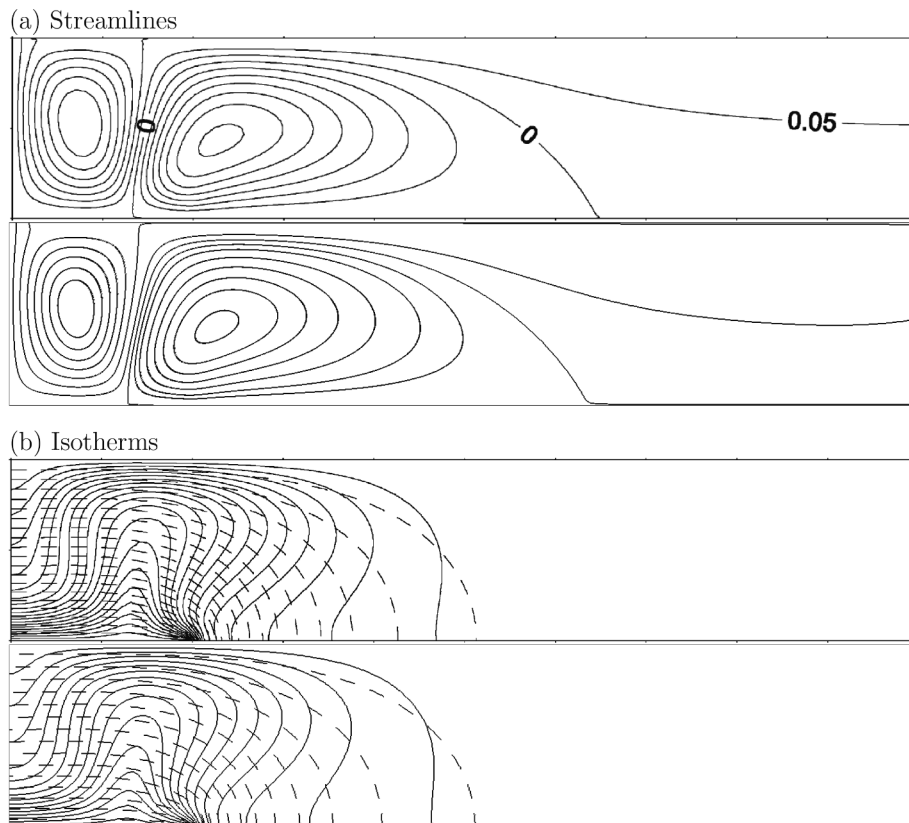


Fig. 5. Numerical results for (a) streamlines and (b) isotherms, of a vertical air jet cooling of a source of heat inside a horizontal channel, at Péclet number $Pe = 10$, predicted by (Top) Wong and Saeid [40] and (Bottom) the current code.

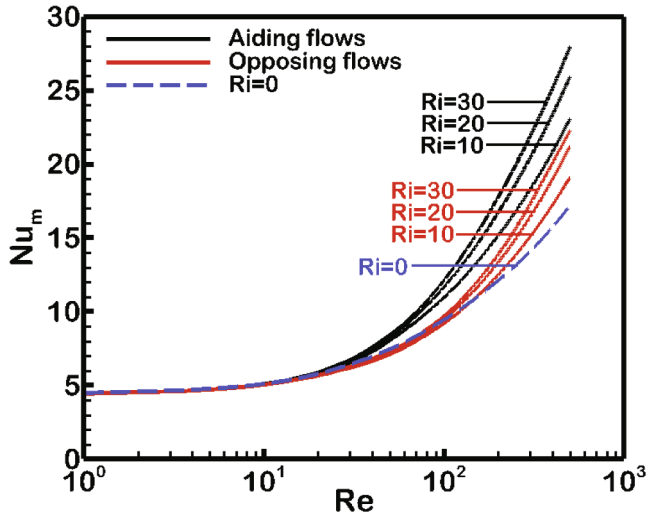


Fig. 6. Variation of mean-time and average-surface Nusselt number with Re for various Ri, for aiding, opposing and pure forced convective flows.

corner of a rectangular cavity and discharging through the other top corner. They found that the positive and negative buoyancies significantly affect the flow and thermal structures in this kind of mixed convective flow configuration. Angirasa [31] examined the intricate interaction among the buoyancy effects and the forced flow inside a square cavity with an entry slot and an exit vent positioned, respectively, at the bottom and the top verges of a vertical wall isothermally heated while keeping the other three walls adiabatic, for various magnitudes of Grashof and Reynolds numbers so that the mixed convection parameter namely, Richardson number, $Ri = Gr/Re^2$, varies within the range of 0.1–10. In fact, the results showed that their numerical algorithm used could not obtain steady-state solutions for higher positive Richardson numbers when the buoyancy effects are dominated. Thus, the periodic flows and unsteady Nusselt number were shown for $Ri \geq 2$. They employed the alternating direction implicit method (ADI) for vorticity-transport and energy equations, and the successive over relaxation technique (SOR) for the stream function equation. Guang et al [32] investigated experimentally and numerically turbulent mixed convection heat transfer in a vertical cavity. They used a liquid nitrogen as a cooling fluid and a mica electronic-heater as a heat source in the experimental work. Whereas, they used three different two-equation models namely, RNG ($k - \epsilon$) model, low Re ($k - \epsilon$) model and SST ($k - \omega$) model, in the numerical simulations employing similar boundary conditions as in the experiments. The focus was to compare the numerical results of the turbulence models with the experimental data, and calculate the average deviations that was found to be all within 25%.

Despite the above-mentioned extensive literature, there seems to be not much research conducted on the case of mixed convection in vertically ventilated enclosures, which is of much relevance to electronic device cooling, and there is still a lack of information about the sophisticated interactions between the buoyancy-induced flow and the pressure-driven external flow within them. Accordingly, the purpose of the current investigation is depended upon the Angirasa [31] configuration for determining numerical solutions to predict the flow and thermal structures within the square enclosure for a broad range of Reynolds number $10 \leq Re \leq 350$ and higher values of Richardson number $0 \leq Ri \leq 30$ using the spectral-element approach that is basically a high-order finite-element method. The concentration is on the characteristics of both opposing and aiding buoyant flows arising from cold and hot upward jets, respectively, and their influences on the recirculating flow and heat removal.

2. Physical description of the problem

The problem of combined forced and free convection heat transfer and fluid flow in a square enclosure is studied in the present numerical investigation. The domain of interest along with the important geometric parameters and the coordinate system used, is displayed in Fig. 1. It consists of a classical geometry of a square enclosure with sides of length H with a slot at the bottom edge of the left vertical wall for the inlet forced flow, and a vent at the top edge of it for the out flow. The inflow slot and the outflow vent are arranged to be opposite each other and fixed at $d = 0.2H$. The buoyancy influences are generated owing to the discrepancy in the temperature between the inflow fluid T_o and the enclosure left vertical wall T_w , while the horizontal and right vertical walls are considered insulated. The wall temperature T_w is kept at either hot or cold temperature, and the incoming flow, which is assumed to be at a constant uniform velocity v_o , is maintained at the ambient temperature T_o , which is also cooler or warmer than T_w .

Indeed, for the flow configuration considered here, the obliged forced flow may assist the buoyant flow or oppose it, relying upon the forced flow direction. Contrariwise, the buoyancy either assists or opposes the forced flow, based upon either the wall temperature T_w is larger or smaller than the temperature T_o of the incoming fluid flow. Hence, the forced flow compelled from the top-down and washing a hotter wall being similar to the flow from the bottom-up above a colder wall. Therefore, it is sufficient to investigate the alteration in the sign of temperature difference, $T_w - T_o$, to be either positive or negative, for producing aiding mixed convective flow when $T_w > T_o$ (cooling effect) or opposing mixed convective flow when $T_w < T_o$ (heating effect), respectively, and keeping the forced flow inlet at bottom.

3. Mathematical formulation

3.1. Governing equations

The working fluid considered in this investigation is air with a Prandtl number of ($Pr = 0.71$). The airflow is deemed to be two-dimensional, transient, incompressible, and newtonian in the laminar flow regime. It is assumed that the fluid physical properties are constant, with the exception of density variation considered in the buoyancy term which follows the approximation of Boussinesq. The energy equation is formulated by neglecting the viscous dissipation and the change of temperature due to compression. Also, the influences of radiation are disregarded, and the gravitational acceleration works in the negative y-direction. Under these foregoing assumptions, the governing conservation equations of mass, momentum, and energy equations can be expressed in the dimensional form as follows:

$$\frac{\partial u}{\partial x} + \frac{\partial v}{\partial y} = 0, \quad (1)$$

$$\rho \left(\frac{\partial u}{\partial t} + u \frac{\partial u}{\partial x} + v \frac{\partial u}{\partial y} \right) = - \frac{\partial p}{\partial x} + \mu \left(\frac{\partial^2 u}{\partial x^2} + \frac{\partial^2 u}{\partial y^2} \right), \quad (2)$$

$$\rho \left(\frac{\partial v}{\partial t} + u \frac{\partial v}{\partial x} + v \frac{\partial v}{\partial y} \right) = - \frac{\partial p}{\partial y} + \mu \left(\frac{\partial^2 v}{\partial x^2} + \frac{\partial^2 v}{\partial y^2} \right) + \rho g \beta (T - T_w), \quad (3)$$

$$\rho c_p \left(\frac{\partial T}{\partial t} + u \frac{\partial T}{\partial x} + v \frac{\partial T}{\partial y} \right) = k \left(\frac{\partial^2 T}{\partial x^2} + \frac{\partial^2 T}{\partial y^2} \right), \quad (4)$$

In order to analyse the thermal and flow fields in general scale, these following scaling parameters are chosen as v_o the average velocity at the inlet, H , the cavity height, $T_w - T_o$, the temperature difference between the hot/cold wall and the inflow, and ρv_o^2 , the characteristic pressure, and the non-dimensional parameters are written as:

$$U = \frac{u}{v_o}, \quad V = \frac{v}{v_o}, \quad X = \frac{x}{H}, \quad Y = \frac{y}{H}, \quad P = \frac{p}{\rho v_o^2}, \quad \tau = \frac{t}{v_o H}, \quad \theta = \frac{T - T_o}{T_w - T_o}, \quad (5)$$

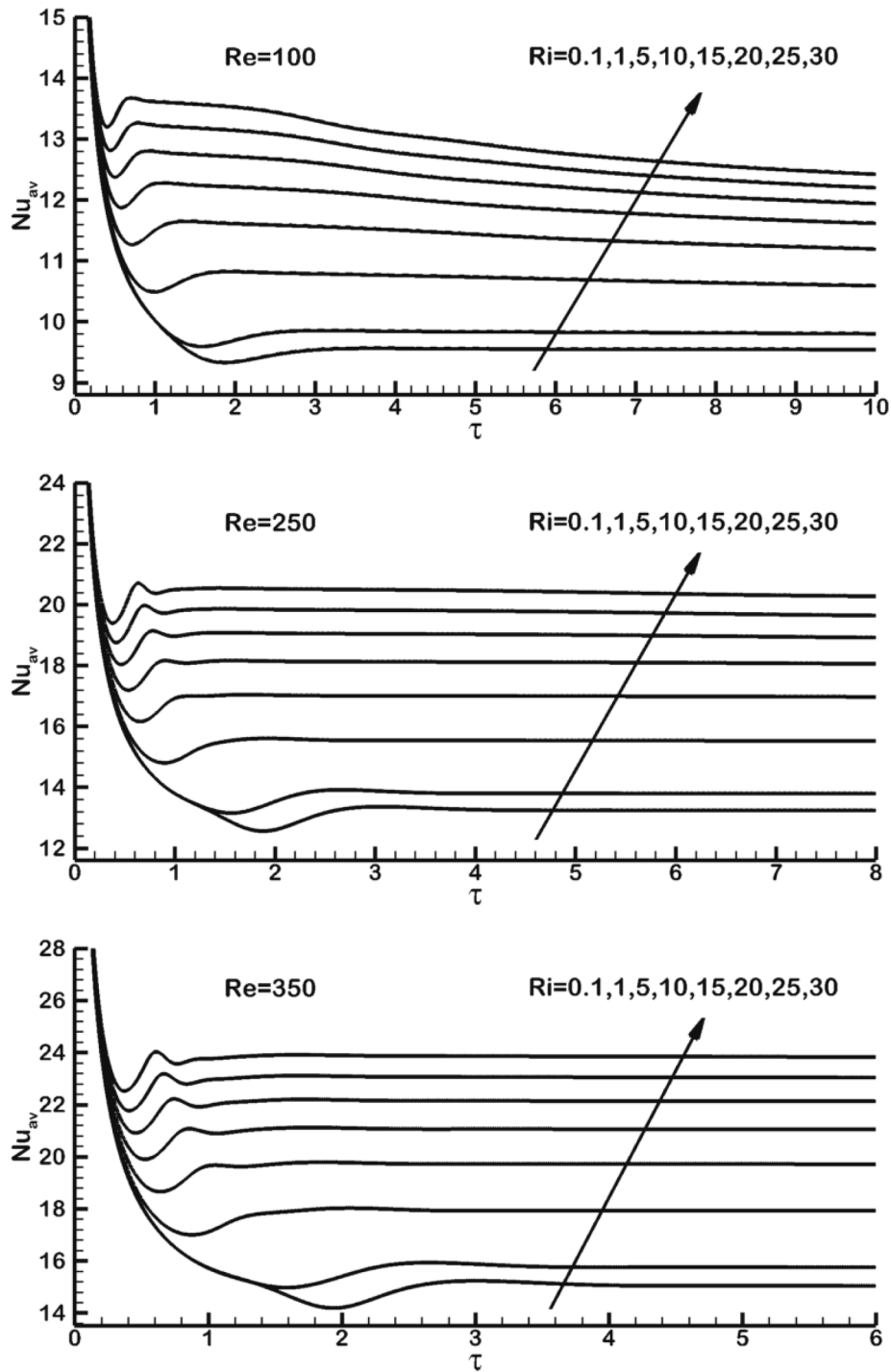


Fig. 7. The evolution of temporal surface-average Nusselt number for different Ri, at Re = 100, 250, 350, for aiding flows.

by the substitution of these parameters in the aforementioned governing conservation equations (1-4), the next non-dimensional equations can be formed:

$$\frac{\partial U}{\partial X} + \frac{\partial V}{\partial Y} = 0, \tag{6}$$

$$\frac{\partial U}{\partial \tau} + (U \frac{\partial U}{\partial X} + V \frac{\partial U}{\partial Y}) = -\frac{\partial P}{\partial X} + \frac{1}{Re} (\frac{\partial^2 U}{\partial X^2} + \frac{\partial^2 U}{\partial Y^2}), \tag{7}$$

$$\frac{\partial V}{\partial \tau} + (U \frac{\partial V}{\partial X} + V \frac{\partial V}{\partial Y}) = -\frac{\partial P}{\partial Y} + \frac{1}{Re} (\frac{\partial^2 V}{\partial X^2} + \frac{\partial^2 V}{\partial Y^2}) + Ri\theta, \tag{8}$$

$$\frac{\partial \theta}{\partial \tau} + (U \frac{\partial \theta}{\partial X} + V \frac{\partial \theta}{\partial Y}) = \frac{1}{Re.Pr} (\frac{\partial^2 \theta}{\partial X^2} + \frac{\partial^2 \theta}{\partial Y^2}), \tag{9}$$

where, U, V represent the dimensionless horizontal and vertical velocity components along X and Y directions, correspondingly; whereas θ, P and τ represent the dimensionless temperature, pressure and time, respectively. The relevant and main governing parameters, which are of interest for the present physical problem as seen in the preceding equations, are Reynolds number (Re), Richardson number (Ri) and Prandtl number (Pr), and are defined as:

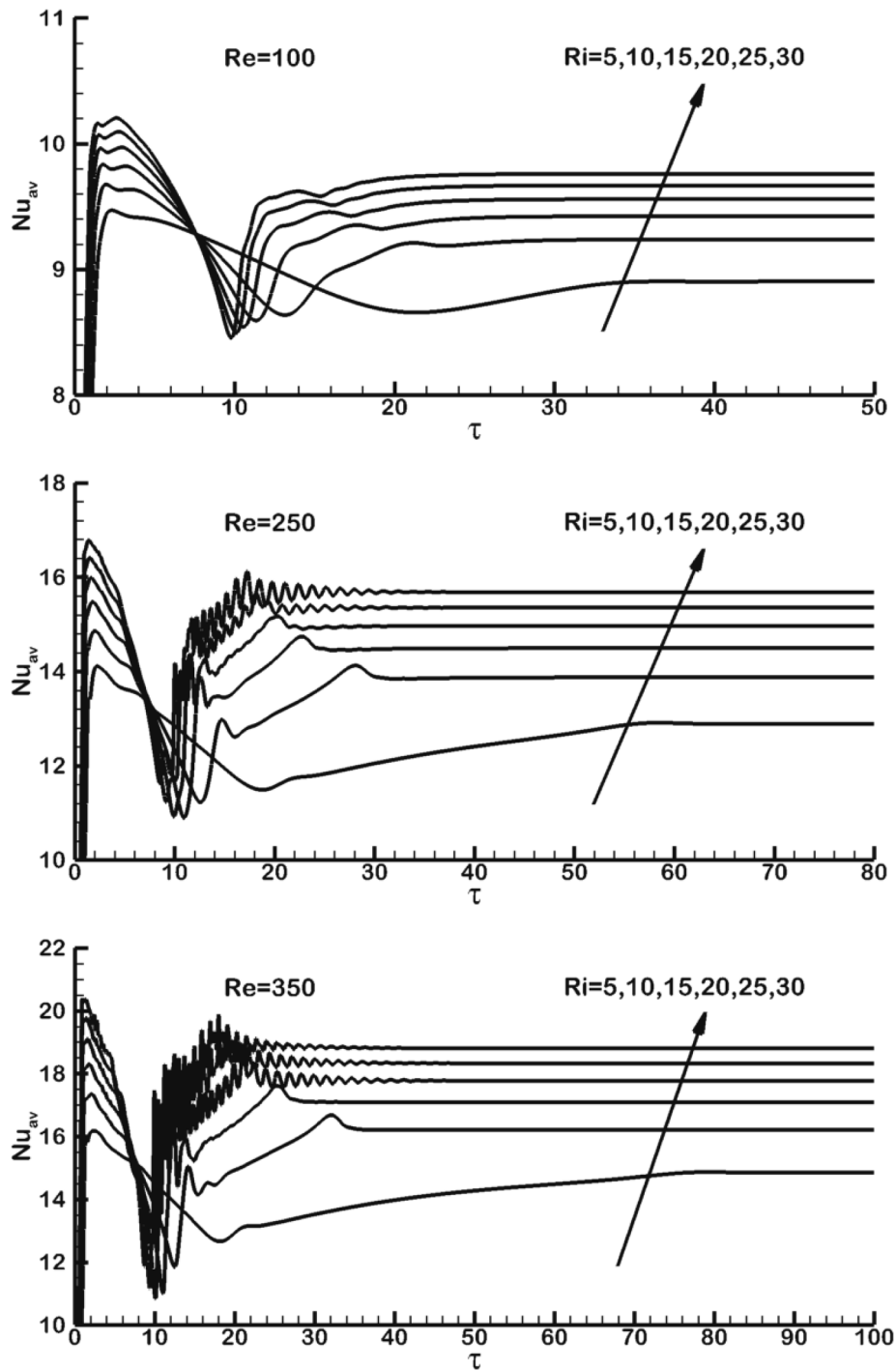


Fig. 8. The evolution of temporal surface-average Nusselt number Nu_{av} for different Ri , at $Re=100, 250, 350$, for opposing flows.

$$Re = \frac{v_0 H}{\nu}, \quad Ri = \frac{Gr}{Re^2}, \quad Pr = \frac{\nu}{\alpha}, \quad Gr = \frac{g \cdot \beta \cdot H^3 (T_w - T_0)}{\nu^2}, \quad (10)$$

where, (Gr) is the Grashof number; α, ν and ρ represent the thermal diffusivity, kinematic viscosity and fluid density, correspondingly, with g and β are the gravitational acceleration and the volumetric expansion coefficient, respectively.

3.2. Boundary conditions

The non-dimensional boundary conditions applied in the current

considered problem are specified as follows:

At the inlet slot, the velocity and temperature are uniform, $U_o = 0, V_o = 1, \theta_o = 0$ for aiding flow, and $\theta_o = 1$ for opposing flow.

At the exit vent, the gradients of all variables in the y -direction are set to zero, $\partial U / \partial Y = \partial V / \partial Y = \partial \theta / \partial Y = 0$.

On the left vertical wall of enclosure, a no-slip boundary condition $U_w = 0, V_w = 0$ indicating that the fluid sticks to the wall, and a uniform temperature $\theta_w = 1$ for aiding the flow, and $\theta_o = 0$ for opposing the flow, are imposed.

On the right vertical and horizontal walls of enclosure, the no-slip condition is also enforced $U = 0, V = 0$, and the gradient of

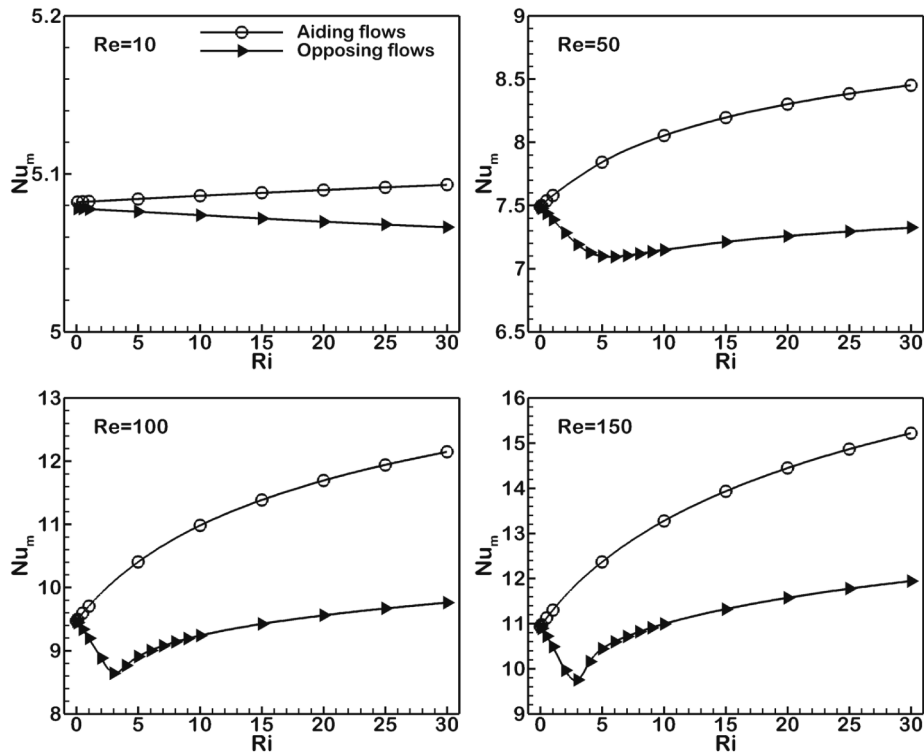


Fig. 9. The variation of Nu_m as a function of Ri for aiding flows, at $Re = 10, 50, 100, 150$.

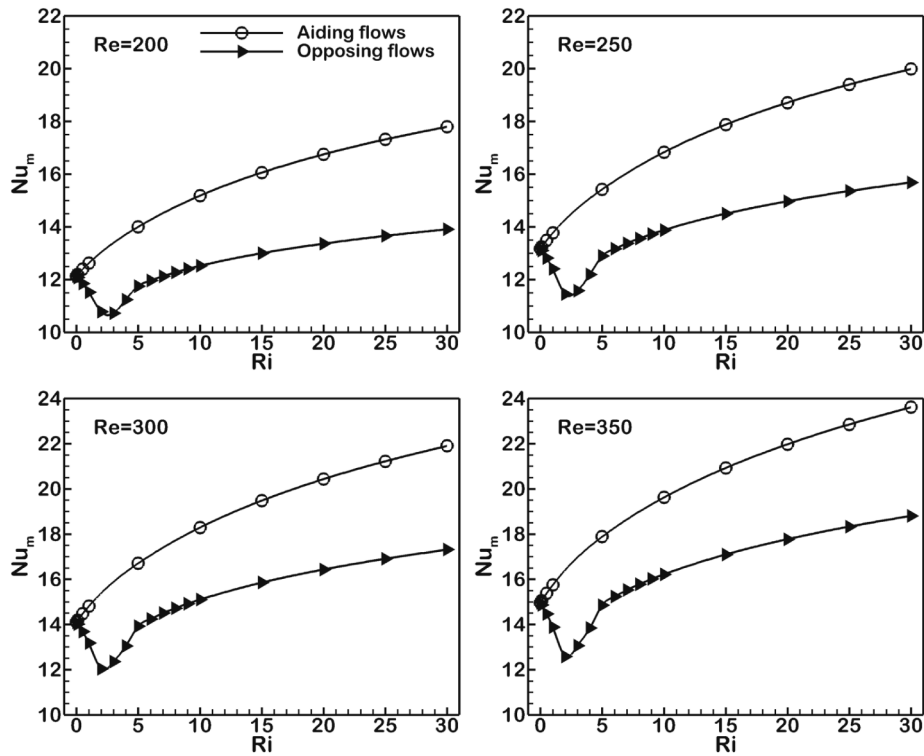


Fig. 10. The variation of Nu_m as a function of Ri for aiding flows, at $Re = 200, 250, 300, 350$.

temperature normal to the walls are set to zero referring to that these walls are insulated.

The flow is assumed to start impulsively from rest.

3.3. Heat transfer characteristics

The exchange of heat between the left vertical wall of enclosure and nearby flowing fluid is calculated in terms of the local surface Nusselt number (Nu_l). As the non-dimensional temperature distribution in the enclosure is computed and becoming well-identified, such

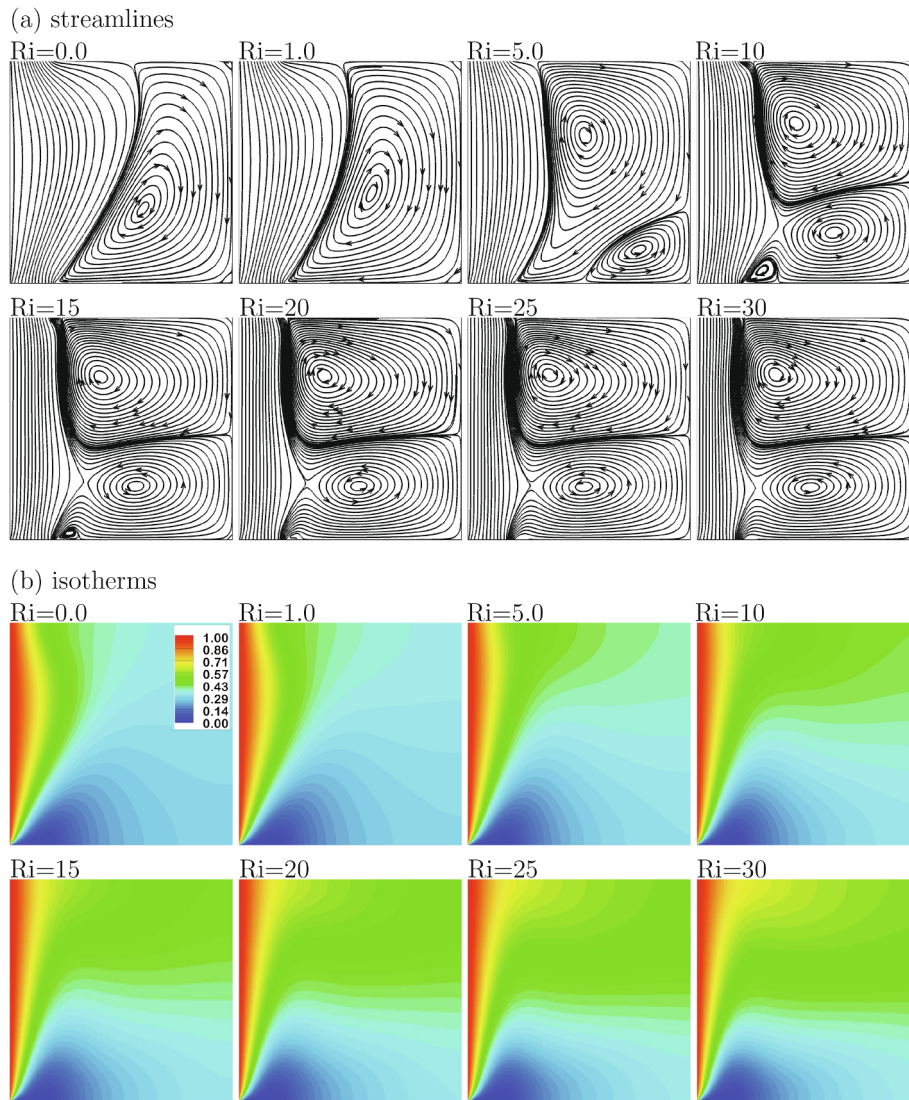


Fig. 11. Patterns of (a) streamline and (b) isotherms, for aiding flows for $Re=50$, and at various Ri .

dimensionless quantity is estimated via this formula:

$$Nu_l = \frac{h_y \cdot Y}{k} = \frac{\partial \theta}{\partial n} \Big|_w, \quad (11)$$

where h_y is the coefficient of local convective heat transfer, n is the direction perpendicular to the wall surface and k is the thermal conductivity of fluid. The surface-average Nusselt number (Nu_{av}) is obtained by integrating the local Nusselt number along the wall.

$$Nu_{av} = \frac{1}{H} \sum \int_0^H Nu_l \cdot dn \quad (12)$$

The time- and surface-average Nusselt number (Nu_m) is calculated via integrating the respective quantities over a large period of time.

4. Numerical procedure

The above equations (6-9), compose the mathematical model to analyse the transport of energy and transient momentum in the unsteady mixed forced and natural convection flow. This is a regime of greatly coupled formulas characterising the development of the main four relevant fields, i.e., horizontal and vertical velocity components U and V , respectively, pressure P and fluid temperature θ . For solving

numerically such system of formulas, it is essential to discretise the problem in both space and time. An existing in-house solver, using the approach of the time-split spectral element, which is characterised by Karniadakis et al. [33] and Thompson et al. [34], was employed to numerically simulate the flow and thermal fields. The temporal discretisation procedure utilised for the current investigation is a scheme of time-splitting with three- and two-steps for momentum and energy expressions, correspondingly. The name of time-splitting for such method is due to that the right-hand side of the equations is split to two or three sets and integrated individually, resulting in the entire integration over one time-step being divided into two or three sub-steps. For equations of momentum, such steps consider the terms of advection, diffusion and pressure. In addition, the sub-steps use a diversity of the temporal discretisation. For instance, an “explicit approach” (Adams-Bashforth) can be employed to handle the advection term owing to its nature of non-linearity, while an “implicit approach” (Adams-Moulton) is used for the sub-steps of diffusion and pressure. This method is comprehensively explained in Karniadakis et al. [33] and Thompson et al. [34].

The technique of the nodal-based spectral-element that is deemed as a “high-order Galerkin finite-element” method, is used as a tool for discretising the controlling equations in space. Within such technique,

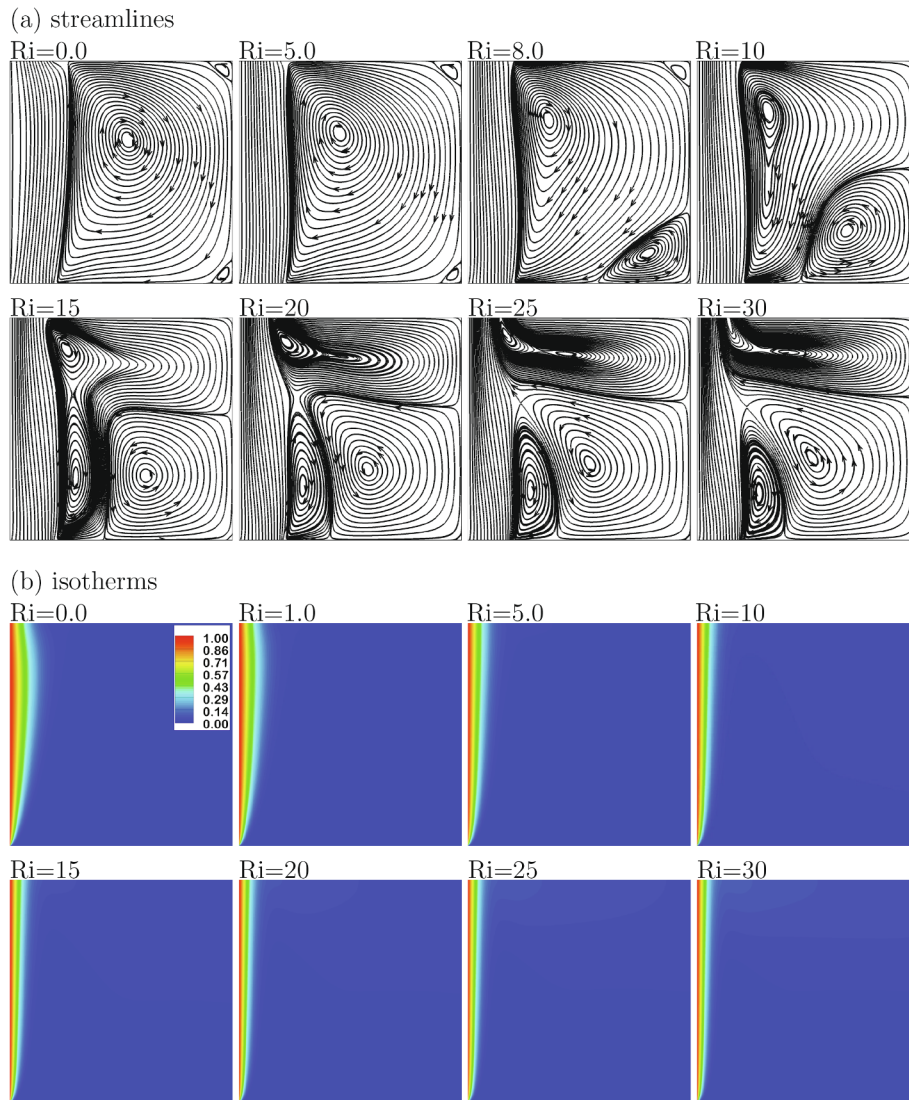


Fig. 12. Patterns of (a) streamline and (b) isotherms, for aiding flows for $Re=350$, and at various Ri .

the spatial domain being normally subdivided roughly into a group of disintegrated macro-elements. The refinement is done for the macro-mesh generated in zones of domain that undergo big gradients (h -refinement). The spatial discretisation used for the computational domain is depended upon quadrilateral elements; despite such elements have the freedom to possess curved sides. In such method, the macro-elements use high-order Lagrange polynomials as weighting and shape functions. These polynomials are related to Gauss-Lobatto-Legendre quadrature points, which results in an effectual calculation of integrals demanded for solving the equations. For increasing the number of points towards more enhancement for the resolution of the computational grid, the order of such polynomials (p) can be raised from 2 to 14. Thus, internally, instead of using a linear basis (e.g. low-order) over each element, each element is subdivided into $(N_x \times N_y)$ nodes permitting a high-order polynomial basis to be instead employed, allowing a very rapid convergence with increasing polynomial degree. Such sort of refinement is recognised as (p -refinement) leading together along with the (h -refinement) stated earlier to a ($h-p$) approach. Indeed, that is the essential benefit of the $h-p$ discretisation method, hence, the numerical domain is discretised one time only with as much as typical macro-element mesh, and later a precisely converged solution is performed via merely rising the polynomial order p at the time of run

till the numerical convergence is achieved. The spatial discretisation treatment employing the Galerkin approach is properly reported by, for instance, Fletcher [35] and Karniadakis and Sherwin [36].

The computational mesh utilised in the current study employs 840 elements macro-elements shown in figure 2(Left). To ensure at what spectral resolution the solution is a grid independent, and consecutively what resolution gives a reasonable compromise between the precision and the calculation expense, a study of grid resolution for the previously mentioned mesh is performed. As explained at the beginning, the interpolants of order ($p = N-1$) being employed for representing the parameters of solution through the spatial discretisation. This results in a group of $(N_x \times N_y)$ internal node points through every macro-element of the mesh, whilst preserving the same layout of macro-element. Accordingly, in the current investigation, the resolution of mesh is changed via varying the order of such interpolants from 3 to 9. Simulations were run at the highest values of Richardson number $Ri = 30$ and Reynolds number $Re = 350$, for both assisting and opposing flows. The local and surface-average Nusselt numbers Nu_l and Nu_m were observed as accuracy indication. Then, the choice of a proper value of p depends otherwise on the range of p for which the solution does not diverge. The results shown in Fig. 3 depict that Nu_l and Nu_m are varied with a relative error of less than 0.5% for polynomial orders from 6 to 9,

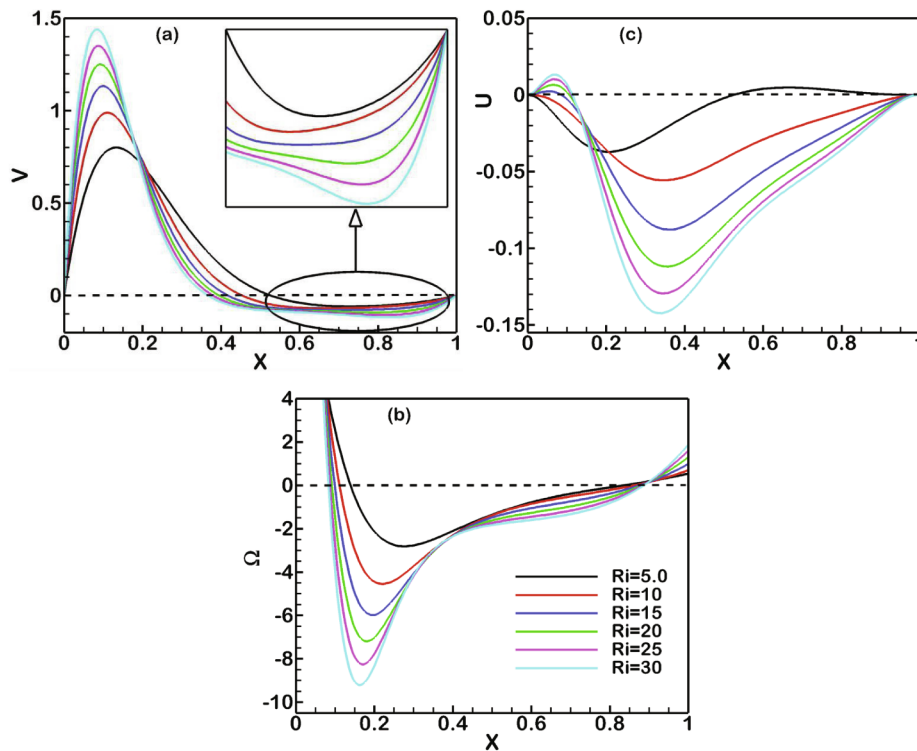


Fig. 13. (a) Vertical velocity, (b) horizontal velocity and (c) vorticity, distributions along the x-direction for aiding flow at $Re=50$, and at various Ri , at $y=0.644$ (the centre location of main vortex at $Ri=5.0$).

for both flow cases. This gives a superior standing of reliance that the results of the present study, employing seventh-order polynomials $p = 7$ ($N_x \times N_y = 8 \times 8$), are adequately resolved. Fig. 2(Right) illustrates the spectral micro-elements mesh used for the simulations.

This solver has been extensively validated previously for many forced convection flow problems such as the flow around a single cylinder (Al-Sumaily and Thompson [37]) and around multi-cylinders (Al-Sumaily [38]), and for free convection flows in a cavity (Al-Sumaily [39]). The solver was modified to incorporate the new equations and flow physics. For the validation of the present implementation of this modified code, results from the code were compared with formerly published numerical results for the problem of mixed convection flow in a ventilated cavity with an isothermal vertical wall conducted by Angirasa [31], and for the problem of a cooling air jet impinging on an isothermal heated surface located in a horizontal channel performed by Wong and Saeid [40].

Figs. 4 and 5 show these comparisons for the streamlines and thermal patterns and the variation of local Nusselt number. A good agreement among the three numerical results can be noted in these figures.

5. Results and discussion

As mentioned before, for the flow configuration considered here, the forced flow is imposed from the bottom-up, and the buoyancy may oppose or assist the forced flow, relying upon if the wall and the inlet fluid temperature difference ($\theta_w - \theta_o$) is positive (+1) or negative (-1). It is essential to test the range of the governing parameters Reynolds number (Re) and Grashoff number (Gr) or Richardson number (Ri) chosen in the present study. Thus, attention is first given to find the region that covers the mixed convection regime. For this propose, many numerical runs were conducted for broad ranges of these pertinent parameters. Typical variations of mean-time and average-surface Nusselt number Nu_m with Reynolds number for various Richardson number are shown in Fig. 6 for both aiding and opposing flows. The

variation for $Ri = 0$ gives, of course, the purely forced convective result. It can be seen that as Reynolds number tends to zero, Nu_m tends to a constant value, the purely free convective limit. It is also seen that for purely forced convection, Nu_m tends to be approximately proportional to $Re^{0.5}$ at higher Reynolds number. In the zone of mixed convection, the general form of the Nu_m variation is expected to be increased above the purely forced convective limit in assisting flows at all Reynolds number as a result of the buoyancy forces. However, in opposing flows, Nu_m is decreased below the purely forced convective limit due to the presence of the buoyancy force at lower Reynolds number, but the values of Nu_m rise above these for the purely forced convection at higher Reynolds number. Accordingly, for the thorough current numerical computations, the Reynolds number is chosen to change between 10 and 350. The Grashoff number is changed indirectly through the ratio of (Gr/Re^2) that is Richardson number (Ri), which is specified with a range of (0–30). The higher Richardson number represents the buoyancy prevalent flow, whereas the lower Richardson number corresponds to the forced convective prevailed flow.

The general transient behaviour of the system characterised by the development of the average Nusselt number Nu_{av} with time is described in Figs. 7 and 8 for both assisting and opposing flows, respectively, for the entire chosen range of Richardson number and at higher values of $Re = 100, 250$ and 350 . These figures reveal that the steady-state solutions can be obtained smoothly and rapidly for aiding flows for all Richardson and Reynolds numbers. However, for opposing flows, the time dependence of Nu_{av} is shown to be quite complicated, particularly for buoyancy dominated flows and at higher Reynolds number. Hence, the unsteady/periodic behaviour is reported and for long computational time but, the steady-state solutions are eventually obtained.

Figs. 9 and 10 illustrate the variation of the time-mean surface-average Nusselt number Nu_m with Richardson number for various values of Reynolds number, and for the two aiding and opposing flows. In general, at lower Reynolds number and/or lower Richardson number, there exists only a little difference in the heat transfer rate between the two negative and positive flows. However, such difference becomes

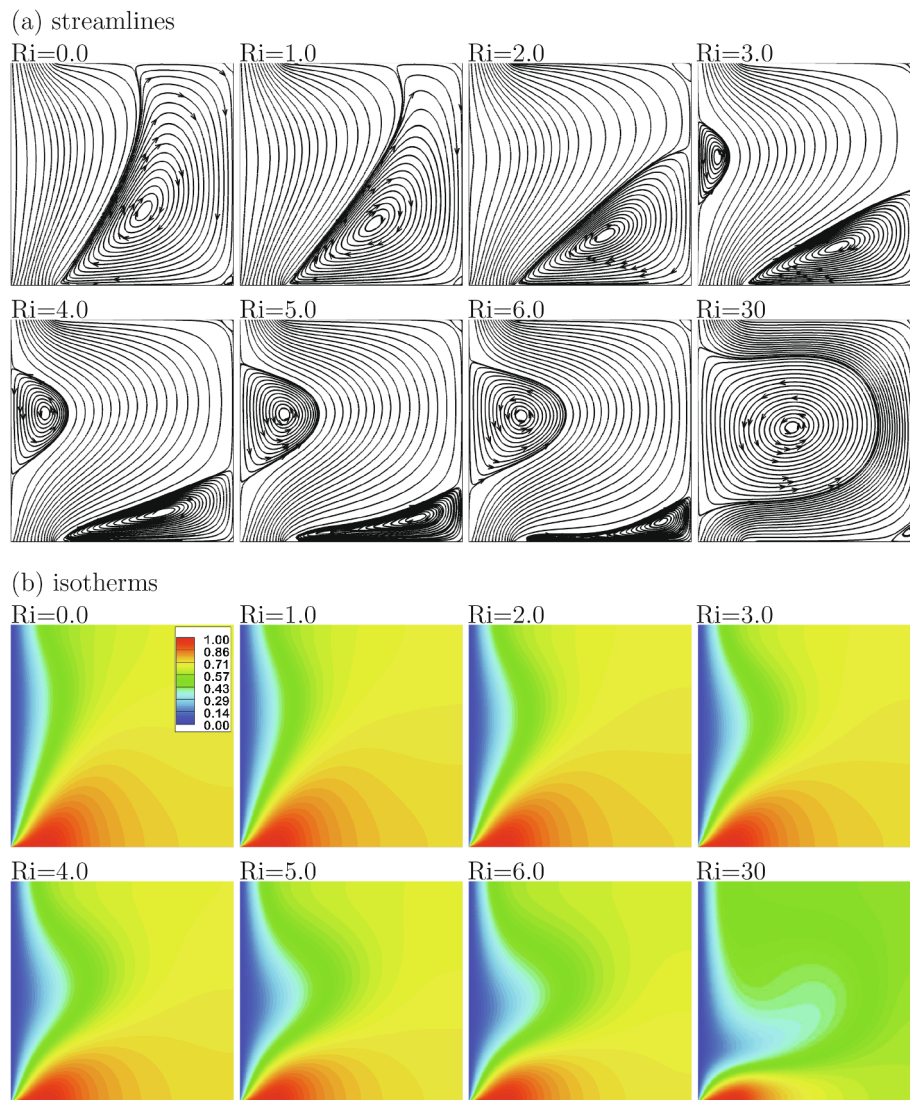


Fig. 14. Patterns of (a) streamline and (b) isotherms, for opposing flows for $Re=50$, and at various Ri .

significant and considerably increases as Richardson number and/or Reynolds number increases. Indeed, higher magnitudes of Nu_m are found within the results of assisting flows, for higher Richardson number and/or higher Reynolds number. Additionally, it is seen that Nu_m increases with increasing Richardson number for all Reynolds numbers in the aiding flows. However, in the opposing flows, the variation of Nu_m depends significantly on the values of Reynolds number and Richardson number. Hence, at $Re = 10$, Nu_m decreases as Richardson number increases. But, for $Re \geq 50$, the figures show that there is a discontinuity in the opposing flow results near the point where Nu_m stops decreasing with increasing Richardson number and starts to rise with increasing Richardson number, e.g. for nearly $Ri > 2$. Thus, the lower and intermediate values of Richardson number result in a lower Nu_m , while the higher Richardson number results in a higher Nu_m , for the same Reynolds number. This is, of course, associated with a switch in the flow patterns from one that is dominated by the forced flow to one that is dominated by the buoyancy forces as will be discussed later. Also, one can see that the forced flow always augments the heat transfer rates for both aiding and opposite flows, Nu_m , thus, raises with raising Reynolds number at similar Richardson number value. The observed changes in the heat transfer rates are all, of course, associated with the alterations in the flow pattern in the cavity.

In order to demonstrate the form of these changes, some typical

streamline patterns and their effect on the temperature distribution are shown in figures (11)-(15), presenting the results at Reynolds number of $Re = 50$ and 350 , for various Richardson numbers $Ri = 0-30$, for both flows. In assisting flow, it can be seen in Figs. 11 and 12 that as Richardson number increases, the intensity of buoyancy forces increases giving rise to a vigorous "upward" flow on the hot vertical wall in the same direction to the forced flow and as a result cause the forced flow to more closely follow the hot wall. The impact of this is to cause an increase in the strength of the recirculating vortex produced within the enclosure, as illustrated in Fig. 13 showing the distributions of the vertical and the horizontal velocities and the vorticity along the x-direction and at

$y = 0.644$ (the centre location of main vortex at $Ri = 5.0$) for $Re = 50$. Also, as Richardson number increases, the single recirculating cell splits into counter-rotating vortex pair at $Re = 50$, and into intricate multiple co- and counter-rotating vortices of varying strength at $Re = 350$. The clear impact may be thought of as thinning of the hydrodynamic and thermal convective boundary layers on the hot wall with a consequent increase in the heat transfer rate.

In the case of opposing flow, the figures concentrate on the changes in the flow and thermal patterns for Richardson number between $Ri = 0-5$, where there is an extraordinary trend of Nu_m for each Reynolds number. Figs. 14 and 15 show that the flow patterns change very

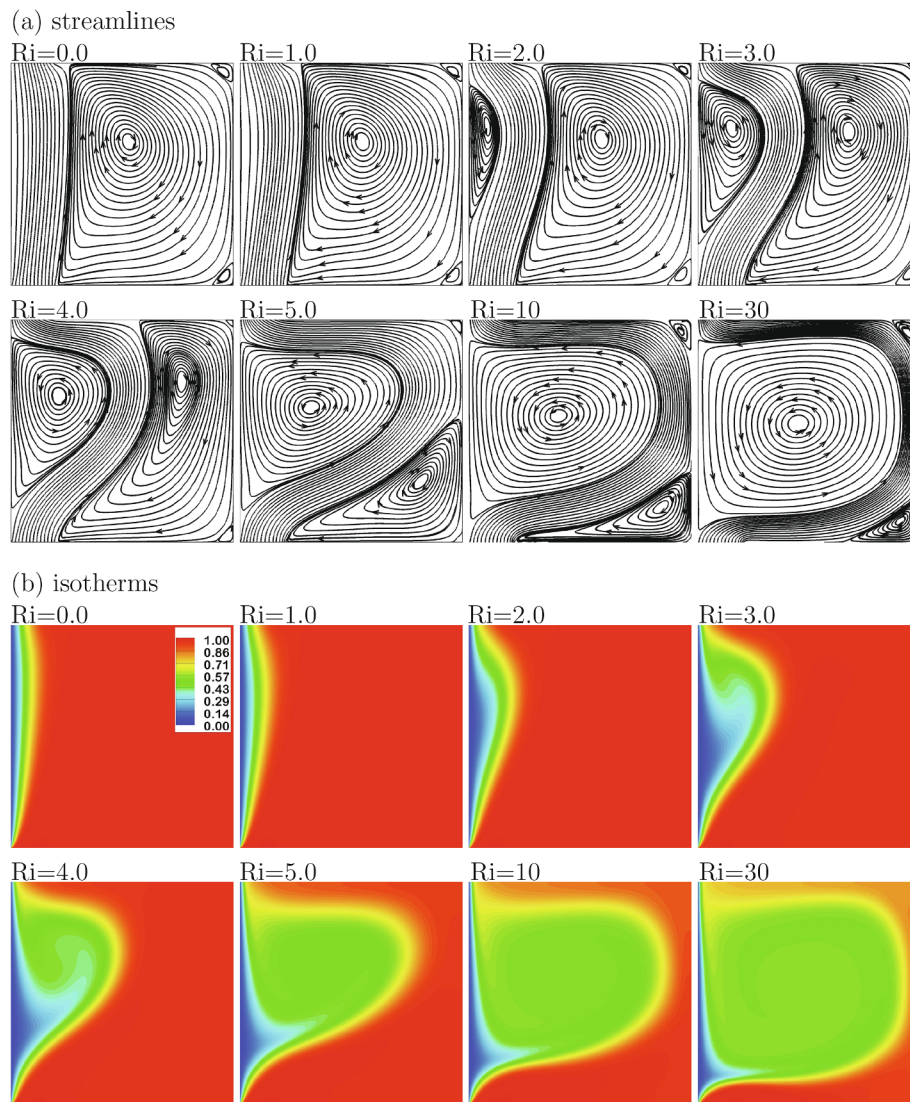


Fig. 15. Patterns of (a) streamline and (b) isotherms, for opposing flows for $Re = 350$, and at various Ri .

significantly. Hence, it is shown that by increasing Richardson number, the buoyancy forces tend to cause a “downward” flow on the vertical cold wall in the opposite direction to the forced flow, and the effect of this conflict is to form a secondary counter-rotating vortex in the vicinity of the cold wall. This buoyancy force driven vortex grows in size as

Richardson number increases, and pushes the forced flow further away from the cold wall and adhering it closely to the opposite perpendicular adiabatic wall, compressing the primary vortex and vanishing it at higher Richardson number. In fact, the sharp drop-rise changes in the mean heat transfer rate Nu_m distribution associated with the formation of the “free convective vortex” on the cold wall take place over a quite narrow Richardson number range of $Ri = 0-5$ in opposing flow.

To analyse the heat transfer attitude more accurately, the typical distributions of the local Nusselt number Nu_l are plotted over the hot and the cold walls and shown in Figs. 16 and 17 for assisting and opposing flows, respectively. Each of these plots gives results for a constant Reynolds number Reynolds number for several values of Richardson number Richardson number. The situation of the assisting flow is firstly regarded and displayed in Fig. 16, where the forced flow

and the buoyancy-induced flow assist each other in enhancing the heat transfer rate. It is demonstrated that the local wall temperature gradients and the values of Nu_l drop sharply from their maximum values close to the inlet slot, and then decrease slightly with further increase in distance along the hot wall towards the outlet vent due to the growth of the boundary layer on this wall. The results display that the distributions have similar a basic form at all Reynolds number and Richardson number with the peak heat transfer rate occurring about one-quarter of the hot wall.

In opposing flow, Fig. 17 illustrates that the local heat transfer rates also reduce from their peak magnitudes close to the forced flow inlet to their minimum values on the lower part of the upright cold wall before starting to considerably increase towards the exit. The position of these minimums moves downward as Richardson number increases due to the downward free convective flow. In addition, with further increasing in Richardson number, a considerable drop in

Nu_l close to the entrance region, however, a sharp change in the variation of Nu_l with a substantial rise in Nu_l is seen with more increase in distance along the cold wall towards the exit. The sharp change in the mean heat transfer rate Nu_m variation with the Richardson numbers in

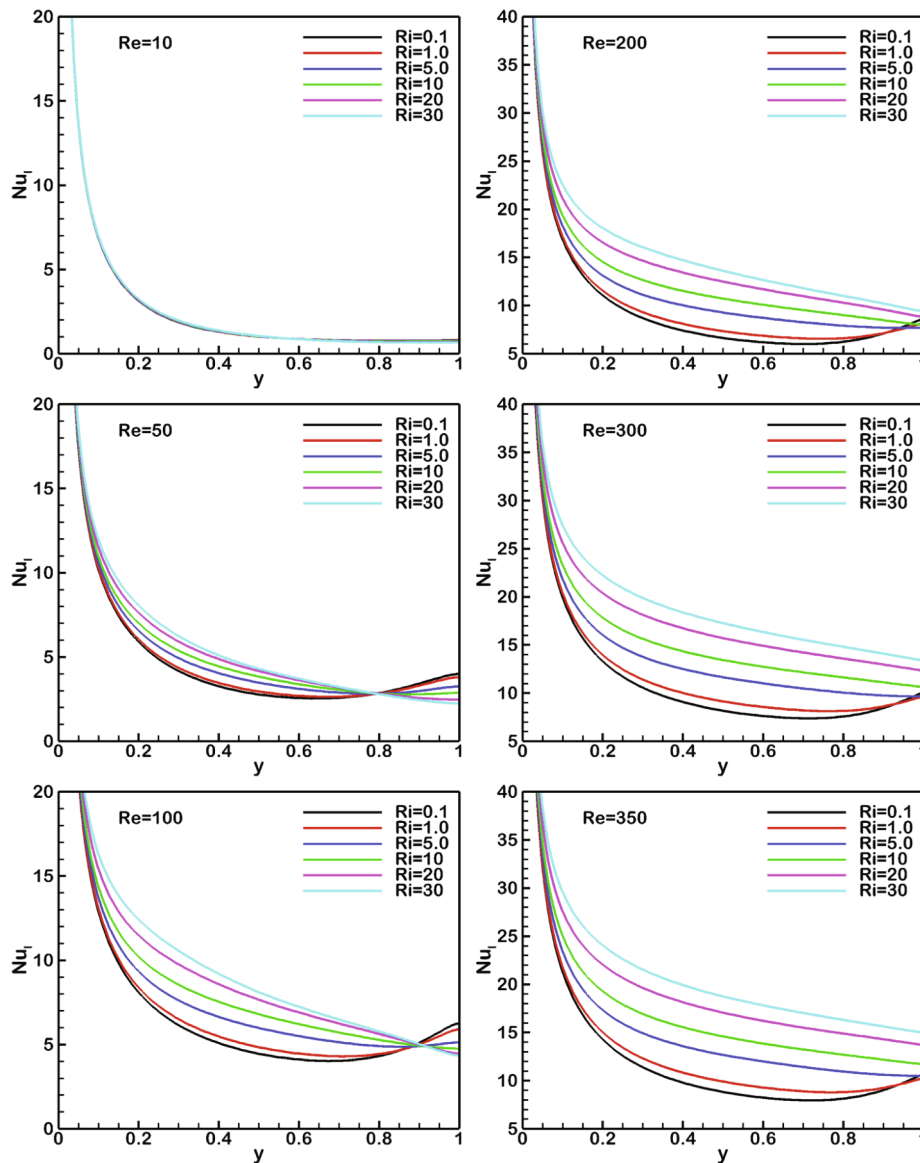


Fig. 16. Time-mean local Nusselt number along the hot wall at various Ri and Re for aiding flows.

the opposing flow mentioned earlier is related to the fairly sharp change in the local heat transfer rate distribution.

6. Conclusion

The present investigation numerically analyses and clarifies the complicated interaction between the buoyancy-induced flow and the pressure-driven external flow in a vertically ventilated square enclosure with an inlet slot and an outlet vent positioned, respectively, down and up of the isothermal vertical left wall, where the remaining three walls are insulated. The influence of changing the Richardson number (Ri) for a broad range of Reynolds number (Re), for both assisting and opposing buoyancies, is examined numerically using the spectral-element method, which is essentially a high-order finite-element method. The following conclusions are drawn from this study: 1. In the assisting buoyancies, the flow prompts a single clockwise vortex, whose intensity relies on the value of Reynolds number, for low Richardson number but,

for the intermediate and high Ri, this primary vortex separates into pair of counter-rotating vortices or multiple co- and counter-rotating vortices depending on Reynolds number. 2. The mean heat transfer rate represented by the mean Nusselt number (Nu_m) is found to be continuously augmented with increasing the buoyancy effect Richardson number and/or the forced flow Reynolds number. 3. However, for opposing buoyancies, fairly large changes in the local and mean heat transfer rate (Nu_l and Nu_m , respectively) distributions occur over a narrower Richardson number range of $Ri = 0-5$, hence, the drop-rise trends for Nu_l and Nu_m variations are shown with minimums at almost $Ri = 2.4$. Importantly, these changes being associated with the formation of the “free convective vortex” in contact with the cold wall generated by the buoyancy force in opposing flow, but the buoyancy forces increase the Nu_m as the purely free convective limit for $Ri > 6.5$. In general, the results manifested that the heat transfer rates of aiding flows are always higher than those of the opposing flows in all circumstances.

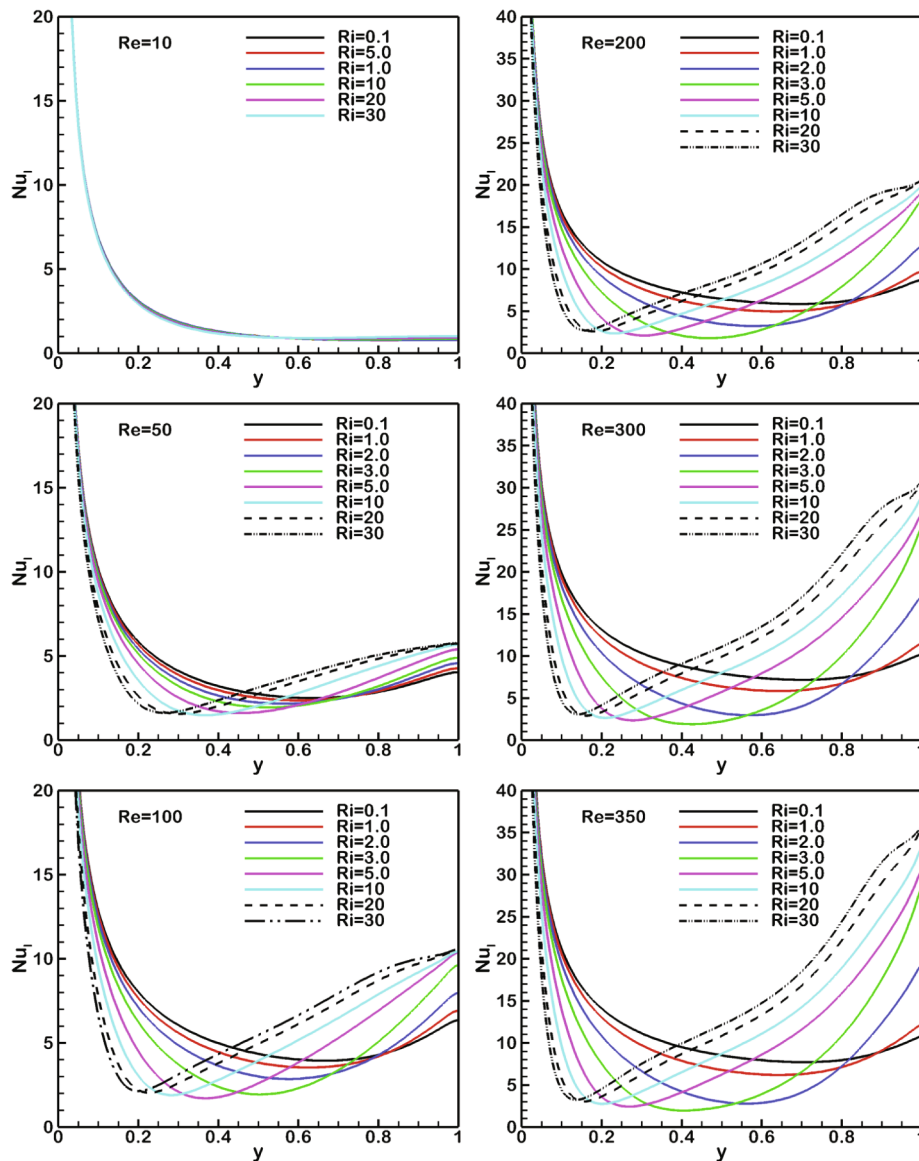


Fig. 17. Time-mean local Nusselt number along the cold wall at various Ri and Re for opposing flows.

Declarations of interest

The authors have no conflicts of interest to declare.

Funding: This research did not receive any specific grant from funding agencies in the public, commercial, or not-for-profit sectors.

Acknowledgement

This research was supported in part by the Monash eResearch Centre and eSolutions-Research Support Services through the use of the MonARCH HPC Cluster.

References

- [1] D. Ramakrishna, T. Basak, S. Roy, I. Pop, A complete heatline analysis on mixed convection within a square cavity: effects of thermal boundary conditions via thermal aspect ratio, *International Journal of Thermal Sciences* 57 (2012) 98–111.
- [2] G. Vinicius, C. Fernando, T. Admilson, L. Silvio, Predictive analytical expression of the Nusselt number for mixed convection in a lid-driven cavity filled with a stable-stratified fluid, *International Journal of Thermal Sciences* 128 (2018) 84–93.
- [3] M. Krunal, H.F. Oztop, E. Mohamed, Mixed convection in a lid-driven cavity containing triangular block with constant heat flux: Effect of location of block, *International Journal of Mechanical Sciences* 152 (2019).
- [4] W. Lei, W. Wei-Wei, C. Yang, L. Di, Z. Fu-Yun, Mixed convection and heat flow characteristics in a lid-driven enclosure with porous fins: Full numerical modelling and parametric investigations, *Numerical Heat Transfer, Part A: Applications* 77 (2020) 361–390.
- [5] H.F. Oztop, I. Dagtekin, Mixed convection in two-sided lid-driven differentially heated square cavity, *International Journal of Heat and Mass Transfer* 47 (2004) 1761–1769.
- [6] S.M. Sebdani, M. Mahmoodi, S.M. Hashemi, Effect of nanofluid variable properties on mixed convection in a square cavity, *International Journal of Thermal Sciences* 52 (2012) 112–126.
- [7] K.K. Ali, G. Shian, Q.A. Ahmed, Unsteady simulations of mixed convection heat transfer in a 3D closed lid-driven cavity, *International Journal of Heat and Mass Transfer* 100 (2016) 121–130.
- [8] D. Youssef, H. Mohammed, A. Abdelkhalik, E. Abdelfattah, H. Safae, Lattice Boltzmann Simulation of Combined Effects of Radiation and Mixed Convection in a Lid-Driven Cavity with Cooling and Heating by Sinusoidal Temperature Profiles on One Side, *Heat Transfer Engineering* 41 (2020) 433–448.
- [9] T.S. Cheng, W.H. Liu, Effects of cavity inclination on mixed convection heat transfer in lid-driven cavity flows, *Computers and Fluids* 100 (2014) 108–122.
- [10] S. Sivasankaran, H.T. Cheong, P. Bhuvaneshwari, M. Ganesan, Effect of moving wall direction on mixed convection in an inclined lid-driven square cavity with sinusoidal heating, *Numerical Heat Transfer, Part A: Applications* 69 (2015) 630–642.
- [11] S. Hussain, S. Ahmad, K. Mehmood, M. Sagheer, Effects of inclination angle on mixed convective nano-fluid flow in a double lid-driven cavity with discrete heat sources, *International Journal of Heat and Mass Transfer* 106 (2017) 847–860.
- [12] Y. Qiang, X. Hang, L. Shijun, Analysis of mixed convection flow in an inclined lid-driven enclosure with Buongiorno's nanofluid model, *International Journal of Heat and Mass Transfer* 126 (2018) 221–236.
- [13] J. Burgos, I. Cuesta, C. Saluea, Numerical study of laminar mixed convection in a square open cavity, *International Journal of Heat and Mass Transfer* 99 (2016)

- 599–612.
- [14] Z. Fatma, M. Zouhaier, E. Afif, B. Ali, L. Patrick, Numerical investigation of entropy generation and heat transfer of pulsating flow in a horizontal channel with an open cavity, *Journal of Hydrodynamics* 29 (2017) 632–646.
- [15] A. Carozza, Numerical Study on Mixed Convection in Ventilated Cavities with Different Aspect Ratios, *Fluids* 3 (2018) 1–18.
- [16] I.I. Nosonov, M.A. Sheremet, Conjugate mixed convection in a rectangular cavity with a local heater, *International Journal of Mechanical Sciences* 136 (2018) 243–251.
- [17] H. Contreras, G. Trevio, J. Lizardi, M. Sustegui, Stereoscopic TR-PIV measurements of mixed convection flow in a vertical channel with an open cavity with discrete heating, *International Journal of Mechanical Sciences* 150 (2019) 427–444.
- [18] T.Y. Duna, A.I. Muneer, Analysis of power law fluid-structure interaction in an open trapezoidal cavity, *International Journal of Mechanical Sciences* 174 (2020) 105–481.
- [19] T.V. Radhakrishnan, A.K. Verma, C. Balaji, S.P. Venkateshan, An experimental and numerical investigation of mixed convection from a heat generating element in a ventilated cavity, *Experimental Thermal and Fluid Science* 32 (2007) 502–520.
- [20] T.V. Radhakrishnan, C. Balaji, S.P. Venkateshan, Optimization of multiple heaters in a vented enclosure - A combined numerical and experimental study, *International Journal of Thermal Sciences* 49 (2010) 721–732.
- [21] A.J. Chamkha, S.H. Hussain, Q.R. Abd-Amer, Mixed convection heat transfer of air inside a square vented cavity with a heated horizontal square cylinder, *Numerical Heat Transfer, Part A* 59 (2011) 58–79.
- [22] E. Papanicolaou, Y. Jaluria, Transition to a periodic regime in mixed convection in a square cavity, *Journal of Fluid Mechanics* 239 (1992) 489–509.
- [23] E. Papanicolaou, Y. Jaluria, Mixed convection from a localised heat source in a cavity with conducting walls: A numerical study, *Numerical Heat Transfer, Part A* 23 (1993) 463–484.
- [24] T. Hsu, P. Hsu, S. How, Mixed convection in a partially divided rectangular enclosure, *Numerical Heat Transfer, Part A* 31 (1997) 655–683.
- [25] A. Raji, M. Hasnaoui, Mixed convection heat transfer in a rectangular cavity ventilated and heated from side, *Numerical Heat Transfer, Part A* 33 (1998) 533–548.
- [26] S. Singh, M.A.R. Sharif, Mixed convective cooling of a rectangular cavity with inlet and exit openings on differentially heated side walls, *Numerical Heat Transfer, Part A* 44 (2003) 233–253.
- [27] M. Zhao, M. Yang, M. Lu, Y. Zhang, Evolution to chaotic mixed convection in a multiple ventilated cavity, *International Journal of Thermal Sciences* 50 (2011) 2464–2472.
- [28] F. Selimefendigil, H.F. Aztop, Numerical investigation and dynamical analysis of mixed convection in a vented cavity with pulsating flow, *Computers and Fluids* 91 (2014) 57–67.
- [29] K. Lounes, Y. Zohir, C. Yassine, N. Hassane, Numerical investigation of turbulent mixed convection in an open cavity: Effect of inlet and outlet openings, *International Journal of Thermal Sciences* 116 (2017) 103–117.
- [30] R. Kumar, T. Yuan, Recirculating mixed convection flows in rectangular cavities, *Journal of Thermophysics and Heat Transfer* 3 (1989) 321–329.
- [31] D. Angirasa, Mixed convection in a vented enclosure with an isothermal vertical surface, *Fluid Dynamics Research* 26 (2000) 219–233.
- [32] Y. Guang, H. Yiye, W. Jingyi, C. Liangjun, Z. and Guozhen, L. Rongrong, C. Aifeng, Experimental study and numerical models assessment of turbulent mixed convection heat transfer in a vertical open cavity, *Building and Environment* 115 (2017) 91–103.
- [33] G. Karniadakis, M. Israeli, S. Orszag, High-order splitting methods of the incompressible navier-stokes equations, *Journal of Computational Physics* 97 (1991) 414–4430.
- [34] M.C. Thompson, K. Hourigan, A. Cheung, T. Leweke, Hydrodynamics of a particle impact on a wall, *Applied Mathematical Modelling* 30 (2006) 1356–1369.
- [35] C.A.J. Fletcher, *Computational techniques for fluid dynamics* Vol. 1 Springer-Verlag, New York, 1991.
- [36] G.E. Karniadakis, S.J. Sherwin, *Spectral/hp methods for computational fluid dynamics*, Oxford University Press, Oxford, 2005.
- [37] G. Al-Sumaily, M.C. Thompson, Forced convection from a circular cylinder in pulsating flow with and without the presence of porous media, *International Journal of Heat and Mass Transfer* 61 (2013) 226–244.
- [38] G. Al-Sumaily, Forced convection heat transfer from a bank of circular cylinders embedded in a porous medium, *Journal of Heat Transfer, ASME* 136 (2014) 042602–042602–11.
- [39] G. Al-Sumaily, Bénard convection from a circular cylinder in a packed bed, *International Communications in Heat and Mass Transfer* 54 (2014) 18–26.
- [40] K.C. Wong, N.H. Saeid, Numerical study of mixed convection on jet impingement cooling in a horizontal porous layer under local thermal non-equilibrium conditions, *International Journal of Thermal Sciences* 48 (2009) 860–870.